LAWRENCE
LIVERMORE
NATIONAL
LABORATORY

LLNL-JRNL-513479

Simplified Metrics for the Identification of the Madden-Julian Oscillation in Models

K. R. Sperber, D. Kim

November 11, 2011

Atmospheric Science Letters

Disclaimer

This document was prepared as an account of work sponsored by an agency of the United States government. Neither the United States government nor Lawrence Livermore National Security, LLC, nor any of their employees makes any warranty, expressed or implied, or assumes any legal liability or responsibility for the accuracy, completeness, or usefulness of any information, apparatus, product, or process disclosed, or represents that its use would not infringe privately owned rights. Reference herein to any specific commercial product, process, or service by trade name, trademark, manufacturer, or otherwise does not necessarily constitute or imply its endorsement, recommendation, or favoring by the United States government or Lawrence Livermore National Security, LLC. The views and opinions of authors expressed herein do not necessarily state or reflect those of the United States government or Lawrence Livermore National Security, LLC, and shall not be used for advertising or product endorsement purposes.

LLNL-JRNL-513479

Simplified Metrics for the Identification of the Madden-Julian Oscillation in Models

Kenneth R. Sperber[1,*] and Daehyun Kim[2]

[1]Program for Climate Model Diagnosis and Intercomparison
Lawrence Livermore National Laboratory
P.O. Box 808, L-103
Livermore, CA, 94550 USA

[2]Lamont-Doherty Earth Observatory of Columbia University
61 Route 9W, Room 201b
Palisades, NY 10964-1000 USA

Atmospheric Science Letters
(Submitted: November 16, 2011
Accepted: March 7, 2012)

*Correspondence to:
K. R. Sperber
Program for Climate Model Diagnosis and Intercomparison
Lawrence Livermore National Laboratory
P.O. Box 808, L-103
Livermore, CA, 94550 USA
E-mail: sperber1@llnl.gov
Ph: 925-422-7720
Fax: 925-422-7675

Short Title: Metrics of the MJO
Keywords: Madden-Julian oscillation; climate models; metrics

Abstract

We propose simplified metrics to evaluate the fidelity with which the Madden-Julian oscillation (MJO) is simulated in climate models. These metrics are based on lag correlation analysis of principal component time series (PC's). The PC's are obtained by projecting simulated 20-100 day bandpass filtered daily outgoing longwave radiation onto the two leading empirical orthogonal functions of observed MJO variability. The simplified MJO metrics, the maximum positive correlation and time lag at which it occurs, provide consistent information relative to more complex diagnostics developed by the Madden-Julian Oscillation Working Group (CLIVAR MJOWG, 2009; Kim *et al*., 2009).

1. Introduction

We are at a unique time in the history of climate modeling, since two comprehensive databases of simulations are openly available to the modeling and analysis communities for understanding processes, validation against observations, and for the assessment of the potential impacts of anthropogenic climate change (Taylor *et al*., In press). The newly available Coupled Model Intercomparison Project-5 (CMIP-5) simulations are just being released and represent the state of the art in climate modeling as of 2011, while the CMIP-3 database represents the capability of models that were available circa 2005.

In the interest of assessing how model performance has changed between these two generations of models, the Working Group on Numerical Experimentation (WGNE) and the CLIVAR Working Group on Coupled Models (WGCM) have established the WGNE/WGCM Climate Model Metrics Panel (http://metrics-panel.llnl.gov/wiki/FrontPage). This panel is seeking recommendations for a standard set of climate and variability metrics for routine application to new climate simulations (it is anticipated that computer code to calculate the simple MJO metrics will be posted on the Metrics Panel website in the near future). These metrics are expected to be easily calculated and understood by a broad community, including non-specialists, and provide an initial indication of the fidelity with which climate and variability are simulated. Given the importance of the MJO in weather and climate variability (e.g., Liebmann *et al.,* 1994; Takayabu *et al.,* 1999) the WGNE/WGCM Metrics Panel asked the Year of Tropical Convection Madden-Julian Oscillation Task Force (YOTC MJOTF) to recommend simple metrics for evaluating the MJO in climate model simulations (Sperber, personal communication, 2011).

The YOTC MJOTF deliberated the appropriateness of candidate metrics through teleconferences and in face-to-face meetings. The ensuing spirited debate prompted the validation of these simple metrics against more complex level-2 diagnostics developed by the CLIVAR MJO Working Group (CLIVAR MJOWG, 2009; Kim *et al*., 2009), including frequency-wavenumber decomposition and Wheeler and Hendon (2004) multivariate EOF's. The goal of this paper is to present simple metrics that capture many of the salient features of the MJO, especially those related to the propagation of convection. The data used in this study are

discussed in Section 2 and the description and application of the metrics is given in Section 3, with Discussion given in Section 4.

2. The Data

In this study we use Advanced Very-High Resolution Radiometer daily outgoing longwave radiation (AVHRR OLR, Liebmann and Smith, 1996) and Global Precipitation Climatology Project (GPCP) daily precipitation (Huffman *et al*., 2001) for November-April 1997-2008. We also use pentad Climate Prediction Center Merged Analysis of Precipitation (CMAP) (Xie and Arkin, 1997) for November-April 1979-2007. OLR is a good proxy of tropical convection (Arkin and Ardanuy, 1989), and has been used in many studies to identify the MJO (e.g., Matthews, 2000; Sperber, 2003; Sperber *et al*., 2005; Matthews 2008).

All data in this study are for the calendar months November-April, when the MJO is typically strongest. The first 15 simulations in Table 1 are from the CMIP-3 Climate of the 20th Century runs for 1961-2000 (model details can be found at: http://www-pcmdi.llnl.gov/ipcc/about_ipcc.php. The following 8 models were evaluated by Kim *et al*., (2009), and consist of three coupled and 5 uncoupled models. One of these models, SPCAM, uses an embedded two-dimensional cloud-resolving model to represent convection and cloud processes. The remaining 4 simulations, sensitivity tests to evaluate MJO sensitivity to changed convective processes, use the Community Atmospheric Model version 3.1 with the Relaxed Arakawa-Schubert convection scheme (CAM3.1/RAS) (Moorthi and Suarez, 1992) and the Geophysical Fluid Dynamic Laboratory Atmospheric Model version 2 (GFDL AM2). The details of the experimental design and further analysis of these two pairs of simulations can be found in Kim *et al*., (2011).

3. MJO Metrics

To aid in understanding and improving the simulation of the MJO, the CLIVAR MJOWG developed a two-tiered set of MJO diagnostics (CLIVAR MJOWG, 2009). Level-1 diagnostics are easy to calculate and provide a preliminary assessment of a models MJO, while the level-2 diagnostics are more comprehensive, and include frequency-wavenumber power spectra and

Wheeler and Hendon (2004) multivariate EOF analysis of near-equatorial OLR, 850hPa and 200hPa zonal wind for testing MJO fidelity. Here we present simple MJO metrics that assess MJO fidelity in a manner consistent with the afore-mentioned more complex diagnostics.

The simple metrics we propose are based on the evaluation of the lag correlation structure of the two principal component time series (PC's) that are associated with the two leading modes of 20-100 day bandpass filtered daily AVHRR OLR. OLR based EOF's have been used extensively in the literature to investigate the dynamical structure and mechanisms of the MJO (e.g., Matthews, 2000; Duffy *et al.* 2003; Sperber 2003; Sperber *et al.* 2005; Matthews, 2008). The two leading modes, shown in Figure 1, were obtained from an Empirical Orthogonal Function (EOF) analysis of filtered OLR using seven winters of strong MJO variability (Sperber, 2003; netCDF files of these EOF's are available at http://www-pcmdi.llnl.gov/projects/ken/mjo_eof/). To ensure a consistent analysis across all models, the 20-100 day bandpass filtered daily OLR from each model is projected onto the observed modes in Figure 1 to obtain their respective PC's. This approach addresses the question of how well the models simulate the observed MJO, and ensures that the metrics are directly comparable with the observations. If a models own EOF's had been used, differences in the spatial patterns would compromise direct comparison of the lag correlation structure of the PC's. Although this simple approach was used in Sperber *et al*. (2005) to evaluate numerous versions of the Max Planck Institute European Centre-Hamburg-4 (ECHAM4) family of models, and by Duffy *et al.* (2003) to evaluate the impact of horizontal resolution on MJO simulation, the usefulness of the simple metrics have not been tested against the more complex level-2 CLIVAR MJOWG diagnostics.

We concentrate on the boreal winter MJO, using PC's for the months November-April, when the MJO tends to be strongest, with eastward propagation of convective anomalies occurring in the near-equatorial region. Figure 2a shows the lag correlation structure of the observed and model PC's. Positive correlation for positive time lag is an indication that PC-2 leads PC-1, consistent with enhanced convection (negative OLR anomalies) propagating from the Indian Ocean to the Maritime Continent. Most of the models (thin colored dashed lines) simulate a lag correlation structure similar to that of the AVHRR OLR (thick black line), though there are several models whose correlation structures are profoundly different from observations.

From the correlation structure in Figure 2a, the simple metrics that we propose consist of the maximum positive correlation and the time lag at which it occurs (Figure 2b and Table 1).

The maximum positive correlation is a measure of how coherent and/or dominant is the propagation of convective anomalies from the Indian Ocean to the Maritime continent. The time lag is the time that it takes for the system to transition from EOF-2 to EOF-1 (Figures 1b and 1a), and it is equal to approximately ¼ of the period of that variability. From observations the maximum positive correlation is 0.69, which occurs at a time lag of 11 days. Compared with observations, all but two models have weaker maximum positive correlations, and for 14/27 models this occurs at time lags of 10-12 days, similar to observations. Four models have their maximum positive correlation at negative time lags, indicating that westward propagation incorrectly dominates in these models. However, the small values of their maximum positive correlations suggest the westward propagation is somewhat incoherent.

Figure 2c shows the frequency-wavenumber power spectra (Hayashi, 1979) of 10°N-10°S averaged GPCP daily precipitation for November-April 1997-2008. This level-2 diagnostic from the CLIVAR MJOWG (2009) and Kim *et al*. (2009) shows the spectral power for eastward vs. westward frequencies (positive frequencies correspond to eastward propagation) for wavenumbers 0-8. For rainfall, eastward propagating power is strongest in the 30-80 day band for wavenumbers 1-3, indicative of the MJO. The East/West power ratio, calculated by dividing the sum of the eastward propagating power by the westward propagating counterpart for the afore-mentioned MJO frequencies and wavenumbers, is a metric used to assess if eastward propagating intraseasonal variability dominates in the MJO band. The East/West power ratios from GPCP, CMAP, and the models, presented in Figure 2d and given in Table 1, indicate that the majority of models underestimate the East/West power ratio, even considering the observational uncertainty of this quantity. An alternative metric is the $East^2$/West power that reflects whether a model over- or underestimates the absolute spectral power (Table 1).

To demonstrate that our simple metric provides information that is consistent with level-2 MJO metrics, we show in Figures 3a and 3b scatterplots of maximum positive correlation vs. the East/West power ratio and the $East^2$/West power for the models and observations. (In instances where a model exhibits westward propagation [maximum positive correlation at a negative time lag], the sign of the maximum positive correlation is made negative to distinguish them from models that have eastward propagation with similar maximum positive correlations). In Figure 3a, the regression fit between the maximum positive correlation and the East/West power ratio for the models is statistically significant at the 5% level for a two-tailed test (correlation = 0.451,

t-value = 2.524). This indicates that the simple metric, the maximum positive correlation, is a good predictor of eastward propagation of MJO convection. However, the regression fit with the $East^2$/West power just misses the 5% significant level (correlation = 0.365, t-value = 1.958), indicating that the maximum positive correlation is not a predictor of MJO amplitude obtained from frequency-wavenumber decomposition (Figure 3b).

Further evidence that the simple metrics are good indicators of MJO fidelity is shown in Figure 4, where we plot longitude-phase plots of filtered OLR that depict the composite life-cycle of MJO convection. These composites are based on the Wheeler and Hendon (2004) multivariate EOF analysis of filtered 15^oN-15^oS averaged OLR, 850hPa and 200hPa zonal wind from observations and a representative set of models. The composites are generated for 8 phases of the MJO life-cycle for days when $(PC\text{-}1^2 + PC\text{-}2^2)^{1/2}$ exceeds 1. Since these composites are generated based on the models multivariate EOF's they provide independent verification that the simple metrics, based on projection of model data onto the observed modes, adequately reflect model performance.

As seen in Figure 4, both AVHRR OLR and CSIRO-Mk3.5 clearly depict the eastward propagation of MJO convective anomalies, consistent with their large maximum positive correlations. INGV-SXG has a smaller maximum positive correlation compared to observations, and this is consistent with its less coherent MJO propagation seen in Figure 4c. Specifically, INGV-SXG exhibits a convective maximum over the Indian Ocean, with weak downstream propagation of anomalies. The GISS-AOM model, Figure 4d, has weak intraseasonal variability with a westward propagation evident, consistent with its small maximum positive correlation occurring at a negative time lag. Figures 4e and 4f evaluate sensitivity simulations that test MJO fidelity relative to a change to the convective parameterization (the so-called Tokioka modification, Tokioka *et al*., 1988) in GFDL AM2. Figure 4f demonstrates that a larger minimum entrainment rate threshold parameter results in a more realistic MJO, since larger entrainment rates are needed to trigger convective plumes. This prevents deep convection from occurring too frequently, which destroys the large-scale organization of tropical convection, such as the MJO.

Additional analysis reveals that the simple metric PC's provide information regarding the magnitude of intraseasonal variability that is captured by the models. The standard deviations of the convective anomalies in Figure 4 are consistent with the PC standard deviations given in

Table 1. Specifically, the CSIRO-Mk3.5 anomalies in Fig. 4b are larger than observed, consistent with the larger than observed standard deviations of PC-1 and PC-2 (Table 1). Similarly, INGV-SXG has weaker but moderate variability (Figure 4c), and GISS-AOM variability is very weak (Figure 4d). The modest increase in the standard deviation of the convective anomalies from GFDL AM2 for Tok =0.1 (Figure 4f) compared to Tok=0.0 (Figure 4e) is also reflected in the PC-1 and PC-2 standard deviations (Table 1). Thus, the results in Figures 3 and 4 indicate that the simple metrics are able to represent the characteristics of simulated MJO's, and they are consistent with results from frequency-wavenumber decomposition and Wheeler and Hendon (2004) diagnostics.

4. Discussion

This investigation promotes the adoption of simple metrics, the maximum positive correlation and the time lag at which it occurs, to perform a preliminary evaluation of boreal winter MJO in models. These metrics are based on projecting model bandpass filtered daily OLR onto observed MJO spatial patterns, and evaluating the lag correlation structure of the resulting PC's. It is demonstrated that there is a statistically significant relationship between the maximum positive correlation and the East/West power ratio obtained from frequency-wavenumber decomposition of near-equatorial precipitation. Additionally, the simple metrics are consistent with MJO fidelity as determined from the composite life-cycle of MJO convection derived from the Wheeler and Hendon (2004) multivariate EOF approach. As such, these simple metrics may be useful as a first-look indication of MJO fidelity by modeling groups and as candidate variability metrics of the MJO for use by the WGNE/WGCM Climate Model Metrics Panel. Since no single metric can be all encompassing with regard to the fidelity of an interaction as complicated as the Madden-Julian Oscillation (MJO), the more comprehensive diagnostics developed by the CLIVAR MJOWG should still be applied to models to perform a more rigorous evaluation of MJO fidelity. These diagnostics include an assessment the vertical structure of the MJO and the processes and dynamical interactions that are known to be associated with a realistic MJO.

The boreal summer intraseasonal variability is more complex, since in addition to the near-equatorial eastward propagation of convection, there is also northward propagation of convection over India and East Asia (Yasunari 1979). This requires that a different domain be

considered for evaluating intraseasonal performance during boreal summer. Sperber and Annamalai (2008) promoted the projection of model data onto observed OLR modes derived from cyclostationary EOF analysis in an evaluation of CMIP-3 model performance. They noted that evaluation of the spatial structure of the model convective anomalies was important for assessing model skill. Thus, quick-look diagnostics for boreal summer intraseasonal variability are not as straightforward as for the boreal winter. Furthermore, alternative approaches for assessing boreal summer intraseasonal variability are being considered, including the use of multivariate spatial EOF's for characterizing the multifaceted intraseasonal dynamics. This issue is the subject of investigation by the YOTC MJOTF through comparing the use of different basis functions to optimize experimental forecast skill.

Acknowledgements

The authors thank the YOTC MJO Task Force (and other invited experts) for their probing questions, insights, critique, and suggestions for validating the simple metrics presented herein. The authors also thank Dr. D. E. Waliser, former co-chair of the YOTC MJOTF, for his support and encouragement in the development of the simple metrics, and for helpful comments on the revised draft. We thank Dr. Matt Wheeler, co-chair of the YOTC MJOTF, for reviewing the submitted and revised versions of this manuscript, and the two anonymous reviewers, whose comments also improved the paper. The MJOTF thanks Dr. Peter Gleckler (PCMDI) and the WGNE/WGCM Climate Model Metrics Panel for their solicitation and guidance in developing the MJO metrics. K. R. Sperber was supported by the Office of Science (BER), U. S. Department of Energy through Lawrence Livermore National Laboratory contract DE-AC52-07NA27344. Daehyun Kim was supported by NASA grant NNX09AK34G.

References

Arkin PA, Ardanuy PE. 1989. Estimating climatic-scale precipitation from space: a review. *Journal of Climate* **2:** 1229–1238.

CLIVAR Madden-Julian Oscillation Working Group. 2009. MJO simulation diagnostics. *Journal of Climate* **22:** 3006-303. DOI: 10.1175/2008JCLI2731.1

Duffy PB, Govindasamy B, Iorio JP, Milovich J, Sperber KR, Taylor KE, Wehner MF, Thompson SL. 2003. High-resolution simulations of global climate, part 1: present climate. *Climate Dynamics* **21:** 371-390.

Hayashi Y. 1979. A generalized method of resolving transient disturbances into standing and traveling waves by space–time spectral analysis. *Journal of the Atmospheric Sciences* **36:** 1017–1029.

Huffman GJ, Adler RF, Morrissey MM, Bolvin DT, Curtis S, Joyce R, McGavock B, Susskind J. 2001. Global precipitation at one-degree daily resolution from multisatellite observations. *Journal of Hydrometeorology* **2:** 36–50.

Kim D, Sperber K, Stern W, Waliser D, Kang I-S, Maloney E, Wang W, Weickmann K, Benedict J, Khairoutdinov M, Lee M-I, Neale R, Suarez M, Thayer-Calder K, Zhang G. 2009. Application of MJO simulation diagnostics to climate models. *Journal of Climate* **22:** 6413-6436 (DOI: 10.1175/2009LCLI3063.1)

Kim D, Sobel AH, Frierson DMW, Maloney ED, Kang IS. 2011. A Systematic Relationship between Intraseasonal Variability and Mean State Bias in AGCM Simulations, *Journal of Climate*, **24:** 5506-5520.

Liebmann B, Smith CA. 1996. Description of a complete (interpolated) OLR dataset. *Bulletin of the American Meteorological Society* **77:** 1275–1277.

Liebmann B, Hendon HH, Glick JD. 1994. The relationship between tropical cyclones of the western Pacific and Indian Oceans and the Madden–Julian oscillation. *Journal of the Meteorological Society of Japan* **72:** 401-412.

Matthews AJ. 2000. Propagation mechanisms for the Madden-Julian oscillation. *Quarterly Journal of the Royal Meteorological Society* **134:** 439-453.

Matthews AJ. 2008. Primary and successive events in the Madden-Julian oscillation. *Quarterly Journal of the Royal Meteorological Society* **126:** 2637-2652 (DOI: 10.1002/qj.224)

Moorthi S, Suarez MJ. 1992. Relaxed Arakawa-Schubert. A parameterization of moist convection for general circulation models. *Monthly Weather Review*, **120:** 978-1002.

Sperber KR. 2003. Propagation and the vertical structure of the Madden-Julian Oscillation. *Monthly Weather Review* **131:** 3018-3037.

Sperber KR, Gualdi S, Legutke S, Gayler V. 2005. The Madden-Julian oscillation in ECHAM4 coupled and uncoupled general circulation models. *Climate Dyn*amics **25:** 117-140.

Sperber KR, Annamalai H. 2008. Coupled model simulations of boreal summer intraseasonal (30-50 day) variability, Part 1: Systematic errors and caution on the use of metrics. *Climate Dynamics* **31:** 345-372. DOI:10.1007/s00382-008-0367-9

Takayabu YN, Iguchi T, Kachi M, Shibata A, Kanzawa H. 1999. Abrupt termination of the 1997-98 El Nino in response to a Madden–Julian oscillation. *Nature* **402:** 279–282.

Taylor KE, Stouffer RJ, Meehl GA. In press. An overview of CMIP5 and the Experiment Design. *Bulletin of the American Meteorological Society* DOI:10.1175/BAMS-D-11-00094.1

Tokioka T, Yamazaki K, Kitoh A, Ose T. 1988. The equatorial 30–60-day oscillation and the Arakawa–Schubert penetrative cumulus parameterization. *Journal of the Meteorological Society of Japan* **66:** 883–901.

Wheeler MC, Hendon HH. 2004. An all-season real-time multivariate MJO index: Development of an index for monitoring and prediction. *Monthly Weather Review* **132:** 1917-1932.

Xie PP, Arkin PA. 1997. Global precipitation: A 17-year monthly analysis based on gauge observations, satellite estimates, and numerical model outputs. *Bulletin of the American Meteorological Society* **78:** 2539–2558.

Yasunari T. 1979. Cloudiness fluctuations associated with the Northern Hemisphere summer monsoon. *Journal of the Meteorological Society of Japan* **57:** 227–242.

Table 1: For Outgoing Longwave Radiation (OLR) the maximum positive correlation for PC-1 vs. PC-2 and the time lag at which it occurred (days) is given for all winters (November-April). For lags greater than zero, non-overlapping time points in each given winter are dropped. Also given are the standard deviations of the PC's, the East/West power ratio, and the East^2/West power (mm^2 day^{-2}) for GPCP precipitation and the models based on frequency-wavenumber decomposition.

	OLR				Precipitation	
Model	R_{max}	Lag (days)	PC-1 std. dev.	PC-2 std. dev.	E/W Power Ratio	E^2/W Power (mm^2 day^{-2})
Obs (1979-2007)	0.69	11	197.81	200.35	2.27	0.29
BCCR-BCM2.0	0.47	15	184.65	205.94	3.73	0.46
CGCM3.1 (T47)	0.30	13	87.14	90.01	1.43	0.06
CGCM3.1 (T63)	0.28	10	87.89	82.79	1.47	0.05
CNRM-CM3	0.43	12	156.44	177.15	6.43	1.00
CSIRO-Mk3.0	0.63	11	188.45	174.92	1.95	0.07
CSIRO-Mk3.5	0.71	10	264.35	246.63	2.84	0.22
GFDL-CM2.0	0.52	12	142.00	153.01	2.43	0.19
GFDL-CM2.1	0.37	12	106.28	108.04	1.93	0.12
GISS_AOM	0.12	-16	32.98	32.65	0.66	0.01
FGOALS-g1.0	0.15	9	74.19	80.19	0.86	0.01
INGV-SXG	0.33	13	141.38	139.92	1.24	0.05
MIROC3.2(medres)	0.33	7	117.87	119.20	1.56	0.05
ECHO-G	0.59	12	251.88	235.87	2.26	0.29
ECHAM5/MPI-OM	0.40	11	174.53	205.29	2.16	0.29
MRI-CGCM2.3.2	0.46	12	146.01	113.21	1.55	0.06
CAM3.5	0.10	-20	160.24	160.37	1.08	0.07
CAM3z	0.53	9	163.78	141.70	2.05	0.20
CFS	0.47	14	163.94	133.02	2.03	0.28
CM2.1	0.28	12	107.76	101.26	1.49	0.11
ECHAM4/OPYC	0.71	10	245.59	216.70	2.25	0.24
GEOS5	0.22	-29	84.84	106.14	1.69	0.09
SNU	0.50	12	157.30	123.88	1.60	0.09
SPCAM	0.57	11	236.12	208.69	2.27	0.30
CAM3.1/RAS (evap=0.05)	0.20	4	118.38	101.84	1.08	0.05
CAM3.1/RAS (evap=0.6)	0.47	10	188.20	152.25	1.63	0.22
GFDL AM2 (Tok=0.025)	0.20	-9	104.08	104.33	0.82	0.04
GFDL AM2 (Tok=0.1)	0.43	13	129.44	105.29	3.05	0.54

Figure Captions

Figure 1. EOF patterns of 20-100 day bandpass filtered AVHRR OLR for winters of strong MJO variability (see Sperber, 2003). (a) EOF-1 and (b) EOF-2. Also given is the percent variance explained by each mode. Positive values are shaded, and negative contours are dashed.

Figure 2. (a) Lead-lag correlation of PC-1 vs. PC-2 over all boreal winters (November-April) from observations (thick black line) and the models (thin dashed lines) with positive time lags corresponding to PC-2 leading PC-1 (Indian Ocean convection leading Maritime Continent convection). (b) Using data from (a) the maximum positive correlation and the day at which it occurs is plotted for the observations (black), the CMIP-3 models (red), and the other simulations (cyan). (c) Frequency-wave power spectrum of GPCP precipitation for November-April ($x10^{-2}$ mm^2 day^{-2}). (d) Bar chart of the E/W power ratios from GPCP, CMAP, the CMIP3 models, and other simulations. The power ratio is calculated for wavenumber 1-3, and periods of 30-80 days (the boxed regions in Figure 2c). Table 1 contains the numerical values of the maximum positive correlations and the E/W power ratios (excepting CMAP whose E/W power ratio = 3.67).

Figure 3. Scatter plots of the maximum positive correlation of PC-1 vs. PC-2 vs. the East/West power ratio (unitless) and the $East^2$/West power (mm^2 day^{-2}) using the data in Table 1. Linear regression fits to the model data are also shown. Observations consist of AVHRR OLR and GPCP precipitation.

Figure 4. Composite longitude-phase plots of 20-100 day filtered near-equatorial OLR (a) AVHRR OLR, (b) CSIRO-Mk3.5, (c) INGV-SXG, (d) GISS-AOM, (e) GFDL AM2 (Tok =0.025), and (f) GFDL AM2 (Tok=0.1). Using the observations and each models own multivariate EOF's the plots are generated for strong MJO's, that is when the normalized amplitude of the PC's $[(PC\text{-}1^2 + PC\text{-}2^2)^{1/2}]$ exceeds 1 for each of eight phases of the MJO, as defined by Wheeler and Hendon (2004). Also given are the maximum positive correlation and the time lag (days) at which it occurs using on the simplified metric (also see Table 1). Inset in each panel is the standard deviation of the longitude-phase OLR anomalies (W m^{-2}).

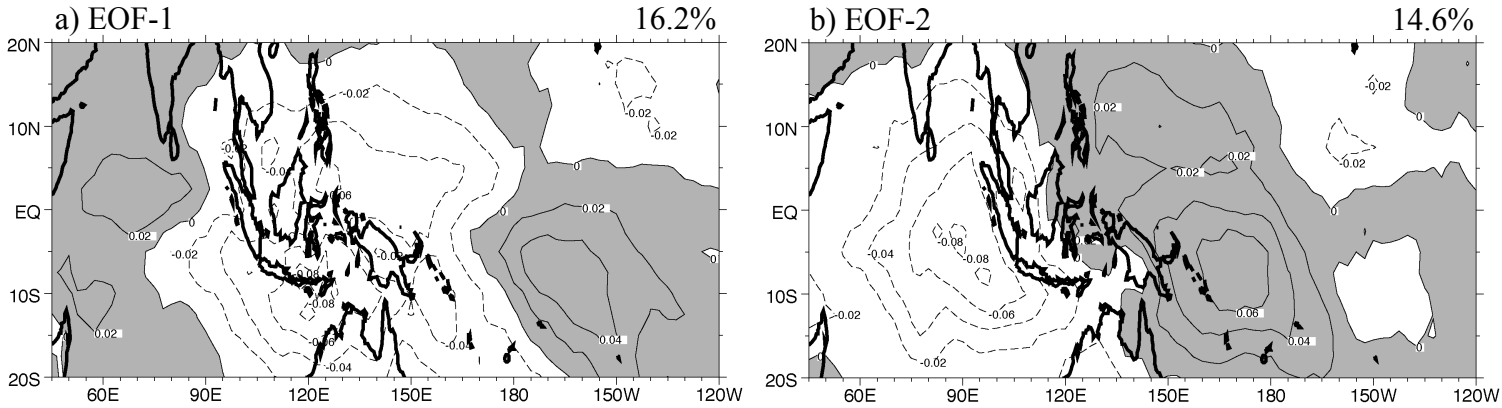

Figure 1. EOF patterns of 20-100 day bandpass filtered AVHRR OLR for winters of strong MJO variability (see Sperber, 2003). (a) EOF-1 and (b) EOF-2. Also given is the percent variance explained by each mode. Positive values are shaded, and negative contours are dashed.

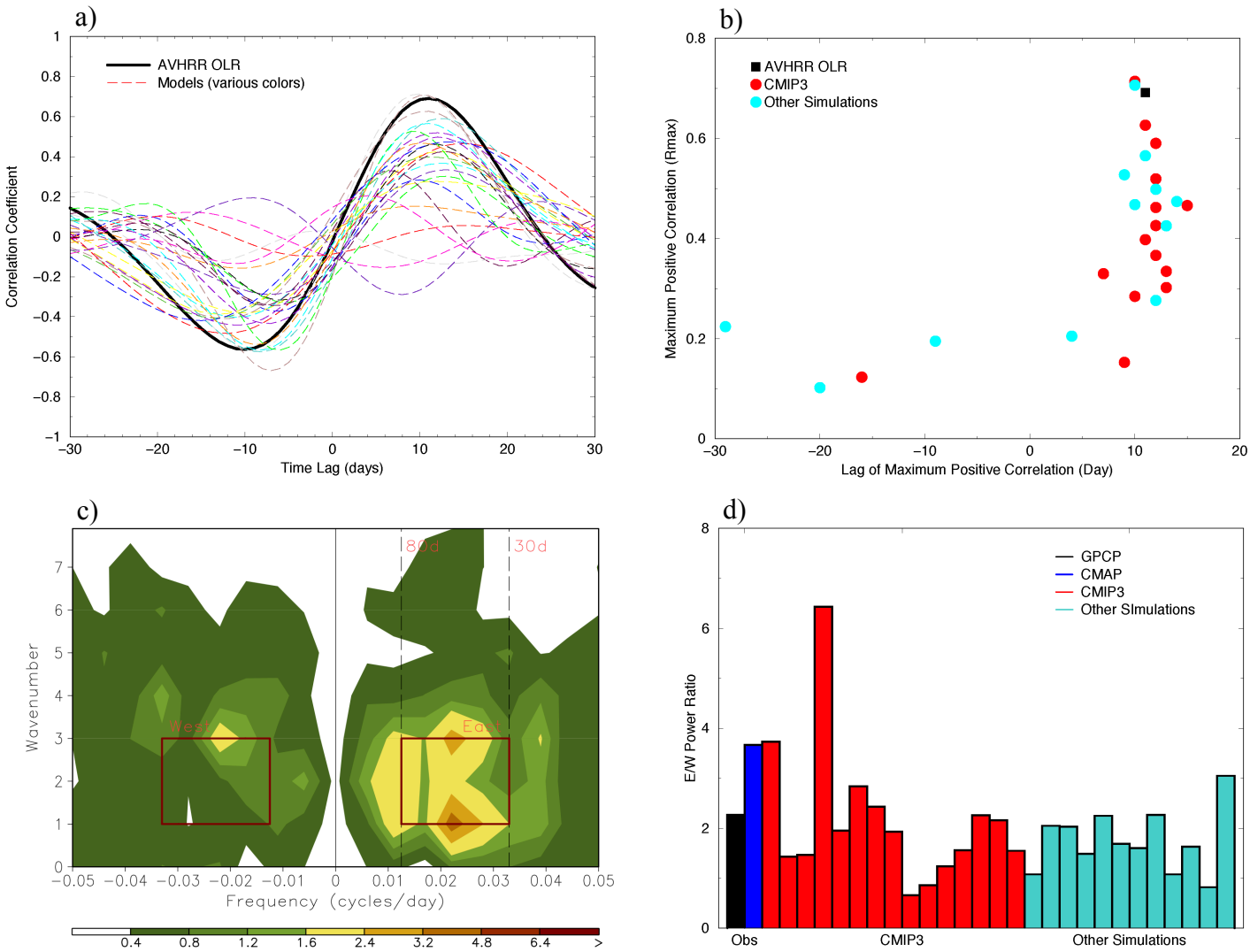

Figure 2. (a) Lead-lag correlation of PC-1 vs. PC-2 over all boreal winters (November-April) from observations (thick black line) and the models (thin dashed lines) with positive time lags corresponding to PC-2 leading PC-1 (Indian Ocean convection leading Maritime Continent convection). (b) Using data from (a) the maximum positive correlation and the day at which it occurs is plotted for the observations (black), the CMIP3 models (red), and the other simulations (cyan). (c) Frequency-wave power spectrum of GPCP precipitation for November-April (x10^{-2} mm^2 day^{-2}). (d) Bar chart of the E/W power ratios from GPCP, CMAP, the CMIP3 models, and other simulations. The power ratio is calculated for wavenumber 1-3, and periods of 30-80 days (the boxed regions in Figure 2c). Table 1 contains the numerical values of the maximum positive correlations and the E/W power ratios (excepting CMAP whose E/W power ratio = 3.67).

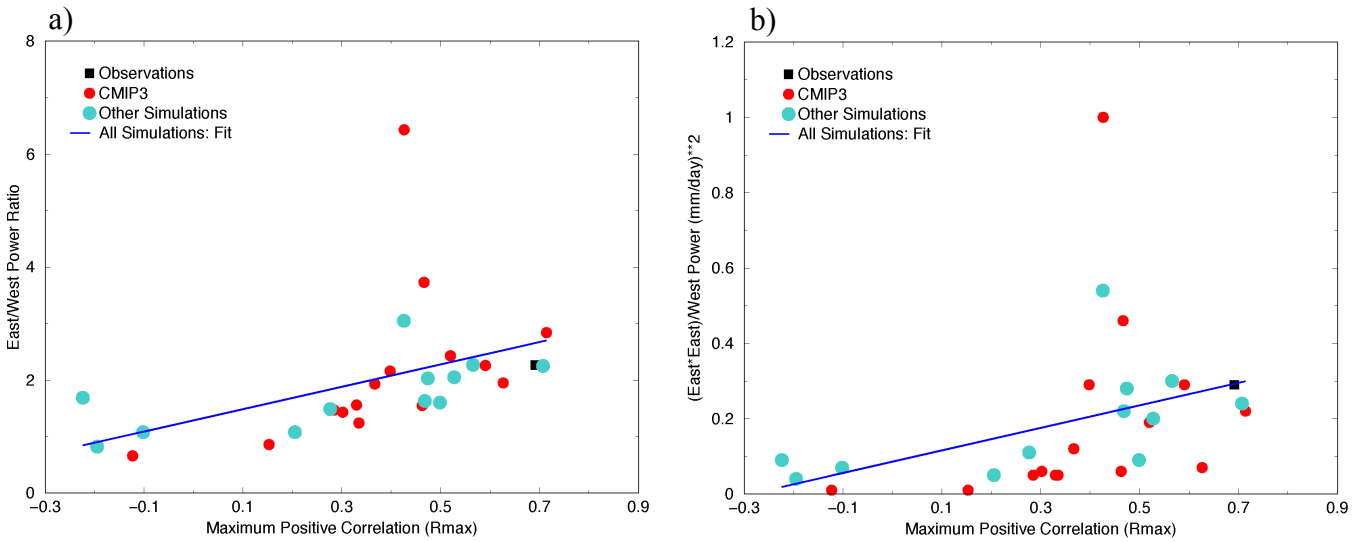

Figure 3. Scatter plots of the maximum positive correlation of PC-1 vs. PC-2 vs. the East/West power ratio (unitless) and the East^2/West power (mm^2 day^{-2}) using the data in Table 1. Linear regression fits to the model data are also shown. Observations consist of AVHRR OLR and GPCP precipitation.

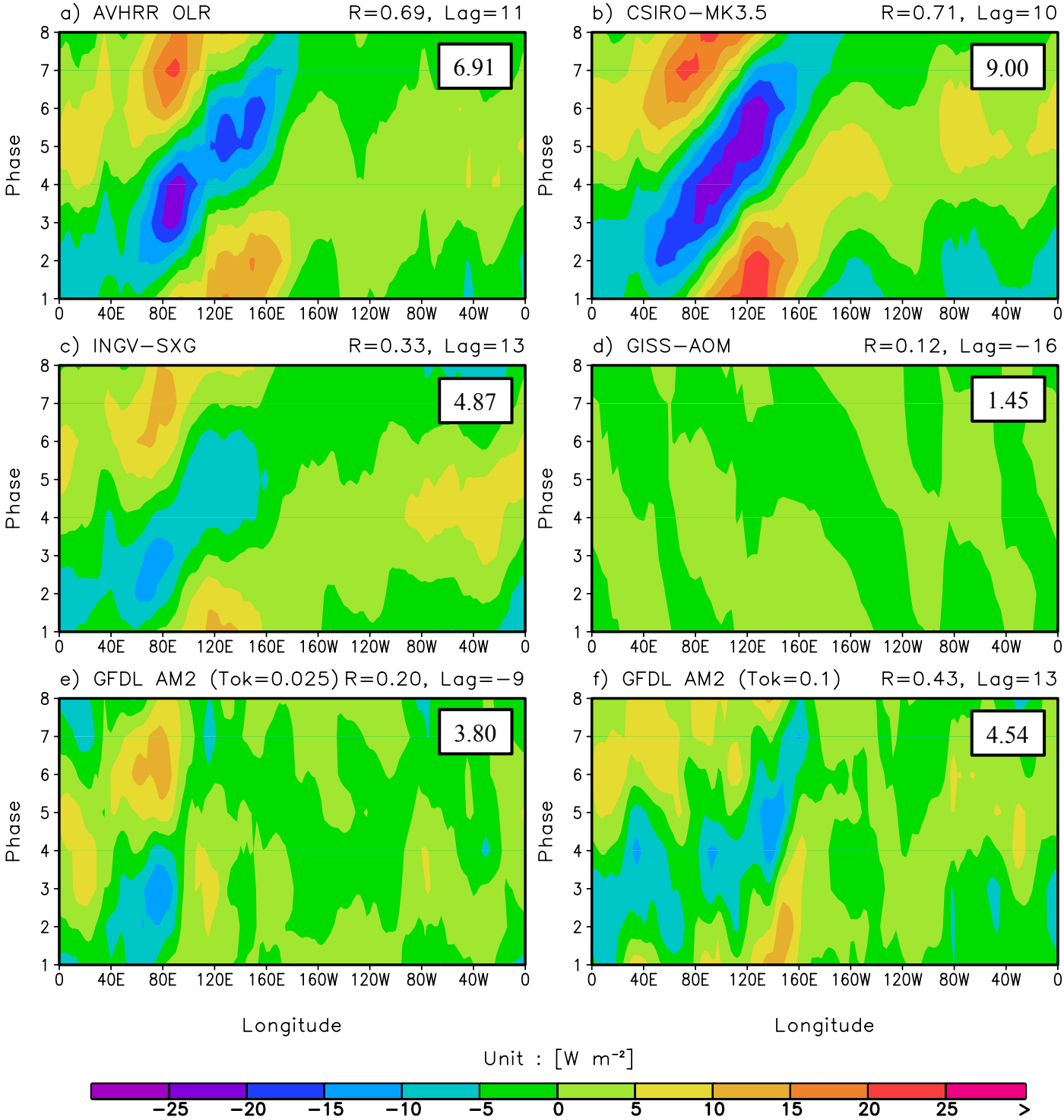

Figure 4. Composite longitude-phase plots of 20-100 day filtered near-equatorial OLR (a) AVHRR OLR, (b) CSIRO-Mk3.5, (c) INGV-SXG, (d) GISS-AOM, (e) GFDL AM2 (Tok =0.025), and (f) GFDL AM2 (Tok=0.1). Using the observations and each models own multivariate EOF's the plots are generated for strong MJO's, that is when the normalized amplitude of the PC's $[(\text{PC-1}^2 + \text{PC-2}^2)^{1/2}]$ exceeds 1 for each of eight phases of the MJO, as defined by Wheeler and Hendon (2004). Also given are the maximum positive correlation and the time lag (days) at which it occurs using on the simplified metric (also see Table 1). Inset in each panel is the standard deviation of the longitude-phase OLR anomalies (W m^{-2}).